Science of the Total Environment 821 (2022) 153292

Contents lists available at ScienceDirect

Science of the Total Environment

journal homepage: www.elsevier.com/locate/scitotenv

Metabolic scaling of stream dissolved oxygen across the U.S. Atlantic Coast

Shakil Ahmed [a,b], Omar I. Abdul-Aziz [a,*]

[a] Department of Civil and Environmental Engineering, West Virginia University, 395 Evansdale Drive, Morgantown, WV 26506-6103, USA
[b] Department of Civil Engineering, East West University, Aftabnagar, Dhaka 1212, Bangladesh

HIGHLIGHTS

- Similitude and scaling of dissolved oxygen (DO) was examined in coastal streams.
- Dimensionless numbers represented the synergistic process controls of stream DO.
- A process diagram revealed high, transitional, and low stream metabolism regimes.
- DO represented a metabolic scaling law in streams across the U.S. Atlantic Coast.
- The scaling law led to a generalized empirical model of DO for coastal streams.

GRAPHICAL ABSTRACT

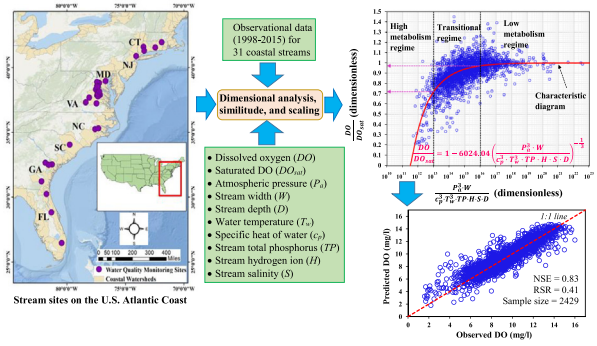

ARTICLE INFO

Article history:
Received 14 August 2021
Received in revised form 16 January 2022
Accepted 16 January 2022
Available online 21 January 2022

Editor: Ashantha Goonetilleke

Keywords:
Dimensional analysis
Predictions
Similitude
Stream metabolism
Water quality

ABSTRACT

We investigated the hypothesis of emergent 'biogeochemical' similitude (parametric reduction) and scaling of dissolved oxygen (DO) in coastal streams across the U.S. Atlantic Coast by employing dimensional analysis methodology from fluid mechanics and hydraulic engineering. Two mechanistically meaningful dimensionless numbers were discovered as the stream 'metabolic' number and the fraction of 'DO saturation' number. The 'metabolic' number represented the synergistic control on stream DO from various climatic, hydrologic, biochemical, and ecological drivers (e.g., water temperature, atmospheric pressure, stream width and depth, total phosphorus, pH, and salinity). A graphical exploration of the 'metabolic' versus the 'DO saturation' numbers led to collapse of data during 1998–2015 from diverse coastal streams into an emergent process diagram, indicating three metabolism regimes (high, transitional, and low). The high and low metabolism regimes were, respectively, characterized by the most and least favorable environmental conditions for stream DO depletion—through reduced dissolution and reaeration, as well as increased organic decomposition, respiration, and nitrification. The emergent process diagram led to a generalized power law scaling relationship of the 'DO saturation' number as a function of the 'metabolic' number (exponent ~ 1/3; Nash-Sutcliffe Efficiency, NSE = 0.83–0.85). The metabolic scaling law was leveraged to develop a generalized empirical model to successfully predict DO in diverse streams across the U.S. Atlantic Coast (NSE = 0.83). The emergent process diagram, metabolic scaling law, and prediction model of DO would help understand and manage water quality and ecosystem health of coastal streams in the U.S. and elsewhere.

1. Introduction

Dissolved oxygen (DO) is crucial for the proper functioning of aquatic ecosystems. It is a key indicator to assess and manage the health of stream water quality and ecosystem (Putro et al., 2016; Li et al., 2017; Zhang et al., 2019; Zhi et al., 2021). However, stream DO is controlled by a multitude of hydroclimatic and biogeochemical drivers having complex interactions—especially in the highly dynamic coastal environments. The intricate interactions among the numerous process drivers pose challenges in achieving a generalized understanding and prediction of stream DO in diverse environmental conditions. Investigations on the synergistic controls of various

* Corresponding author.
E-mail address: oiabdulaziz@mail.wvu.edu (O.I. Abdul-Aziz).

http://dx.doi.org/10.1016/j.scitotenv.2022.153292

biogeochemical and ecological processes on stream DO can help assess stream metabolism, environmental regimes, and ecosystem health across large spatiotemporal scales.

The major processes of enriching stream DO (i.e., sources) are diffusion and reaeration through air-water oxygen mass transfer and photosynthesis by the aquatic autotrophs (Correa-González et al., 2014; Dick et al., 2016). The reaeration rate of DO in water typically depends on the stream velocity, width, depth, and cross-sectional area (Chapra, 2008; Hondzo et al., 2013; Gonçalves et al., 2017). In contrast, the major processes of depleting stream DO (i.e., sinks) are stream nutrient enrichment, nitrification, respiration, and photo-oxidation (Correa-González et al., 2014; Xu and Xu, 2016; Blaszczak et al., 2019; Gu et al., 2020; Johannsson et al., 2021). High temperature can decrease stream DO as a result of increasing decomposition, heterotrophic respiration, and nitrification by stimulating microbial activities (Jabiol et al., 2020). However, temperature effect on stream DO mainly results from the thermodynamic property of water, which leads to a reduced solubility of oxygen gas with an increasing temperature (Chapra, 2008; Ni et al., 2019). The solubility of oxygen decreases with the lower atmospheric pressure at the higher elevations (Girard, 2013). High salinity also leads to an increase of electrolytes (free ions) in stream water, resulting in a reduced solubility of oxygen gas (Garcia and Gordon, 1992). Furthermore, salinity can impact stream DO by creating photosynthetic stress and controlling biogeochemical reactions in aquatic environments (Zhang and Huang, 2011; Berger et al., 2019; Entrekin et al., 2019).

The production and consumption of DO by various stream processes are inherently linked with stream metabolism (Bernhardt et al., 2018; Appling et al., 2018). Previous studies provided important insights into the effect of various environmental drivers on stream metabolism at different spatiotemporal scales (Appling et al., 2018; Bernhardt et al., 2018; Koenig et al., 2019; Savoy et al., 2019; Kindley, 2021; Ledford et al., 2021; Segatto et al., 2021). Appling et al. (2018) presented site-specific models to estimate ecosystem metabolism and DO changes in 356 streams and rivers across the U.S. Ledford et al. (2021) analyzed DO data and reported a high spatiotemporal variability in metabolic regimes of an urban stream receiving effluent discharges from wastewater treatment plants in Philadelphia, USA. Further research is needed to develop a generalized understanding, characterization, and prediction of stream DO, metabolism, and ecosystem health amid the high spatiotemporal variability within and across regions.

Coastal streams provide a wide range of ecosystem services and economic benefits. Apart from flood control, tourism, and recreation, coastal streams provide crucial habitats for diadromous fish species which migrate between the sea and freshwater during their lifecycle (Thuesen et al., 2011; Mitsuo, 2017). Further, coastal streams offer important habitat areas for the growth of certain salmonid species (Rosenfeld et al., 2002; Mitsuo, 2017). However, these streams are at a high risk of water pollution and subsequent deoxygenation due to their highly dynamic nature under a rapidly expanding development pressure (Mahaffey et al., 2020). Much research has reported excess nutrient-driven eutrophication and high temperature as the primary causes for depletion of DO in coastal streams and bays. Previous studies underlined the predominant negative control of water temperature on coastal stream DO in various parts of the world (e.g., Shrestha and Kazama, 2007; Jacobs et al., 2009; Schaefer and Hollibaugh, 2017; Diamantini et al., 2018). Tyler et al. (2009) found that the longest periods of severe hypoxia in the Delaware Coastal Bays had been linked with the higher temperature alongside other abiotic factors (e.g., low insolation, high streamflow). Diamantini et al. (2018) reported increasing temperature as an important factor of DO depletion in various coastal rivers of Europe. Furthermore, increased phosphorus in stream may cause eutrophication (Wang and Linker, 2009; Abdul-Aziz and Ahmed, 2017; Wurtsbaugh et al., 2019; Poikane et al., 2021), which typically results in higher turbidity and oxygen demanding waste to reduce DO (Järvenpää et al., 2019; Mahaffey et al., 2020). Dodds (2006) reported that the nutrient (nitrogen, phosphorus)-enriched runoff from the Mississippi River Basin had been a potential cause of DO depletion in the northern Gulf of Mexico, USA. Wan et al. (2014) reported a strong negative linkage of DO with nutrients (PO_4–P, NH_4–N, and total phosphorus) in the canals of the southern Indian River Lagoon Watershed, Florida. Overall, the existing studies on coastal stream DO mostly focused on local scale, and often did not incorporate the gradients and varying interactions of biogeochemical and hydroclimatic drivers across a large spatial scale.

An important research question is whether the complex interactions of the major process drivers of DO in coastal streams can be combined together to discover emergent similitudes (parametric reductions) and scale-invariant patterns. How is stream DO relatively and collectively controlled by the interacting source versus sink processes? Similitude and dimensional analysis from fluid mechanics and hydraulic engineering (Kundu and Cohen, 2004) can help formulate a small set of dimensionless numbers and achieve emergent similitude by combining important hydroclimatic, biochemical, and ecological drivers of DO in coastal streams (Abdul-Aziz and Ahmed, 2019). The dimensionless numbers can then lead to generalized scaling of DO in coastal streams across space and time (Miragliotta, 2011; Hondzo et al., 2013; Gonçalves et al., 2017). Our current study is motivated by the knowledge gaps in potential similitude, emergent patterns, and generalized scaling of stream DO under diverse coastal environments across a large spatiotemporal scale.

Classical examples of similitude-based generalized process diagrams and scaling relationships are the 'Moody diagram' for pipe flow design (Finnemore and Franzini, 2002) and 'Shields diagram' for characterizing river sediment transport (Hager, 2018). Several studies have employed similitude and dimensional analysis to investigate the interactions of various environmental process components (both biotic and abiotic) in aquatic environment and modeling of stream water quality. For instance, Abdul-Aziz and Ahmed (2019) employed dimensional analysis to evaluate the dominant environmental controls of water quality in coastal-urban streams of southeast Florida. Schwefel et al. (2017) formulated dimensionless numbers and scaling relationship to estimate the dissolved oxygen flux and distribution at the sediment-water interface of Lake Geneva. Warnaars et al. (2007) investigated the interactions of stream biotic and abiotic factors employing similitude and dimensional analysis in various streams and rivers across North America. Hondzo et al. (2013) applied dimensional analysis to study the control of photosynthesis, respiration, advection, dispersion, and aeration processes on dissolved oxygen mass balance in the Minnehaha Creek, Minnesota. Zeleňáková et al. (2013) formulated water quality model by employing dimensional analysis to estimate nutrient concentrations from the hydrologic and climatic drivers in the River Laborec of eastern Slovakia.

The aim of this study is to investigate similitude (parameter reduction), emergent pattern, and metabolic scaling of DO in coastal streams. The underlying research hypothesis is that DO represents emergent 'biogeochemical' similitude and scaling relationship across diverse coastal streams. Dimensional analysis was employed to formulate meaningful dimensionless numbers, incorporating various environmental processes. The dimensionless numbers were computed using observational data and scatterplotted to unravel the emergent patterns and a characteristic process diagram. A generalized scaling relationship of DO was then estimated for diverse coastal streams, incorporating gradients across the Atlantic Coast of USA.

2. Materials and methods

2.1. Study sites and datasets

We included 31 stream water quality monitoring sites located in NOAA's coastal watersheds across the Atlantic Coast of USA (Percy Pacheco, personal communications, 2016) (Fig. 1, Tables S1 and S2). The study sites and period (1998–2015) were selected based on the availability of reliable data, incorporating seasonal and multi-year temporal gradients of stream water quality variables. The large geographical extent encompassed eight U.S. states: (i) Connecticut (CT), (ii) New Jersey (NJ), (iii) Maryland (MD), (iv) Virginia (VA), (v) North Carolina (NC), (vi) South Carolina (SC), (vii) Georgia (GA), and (viii) Florida (FL). The study area

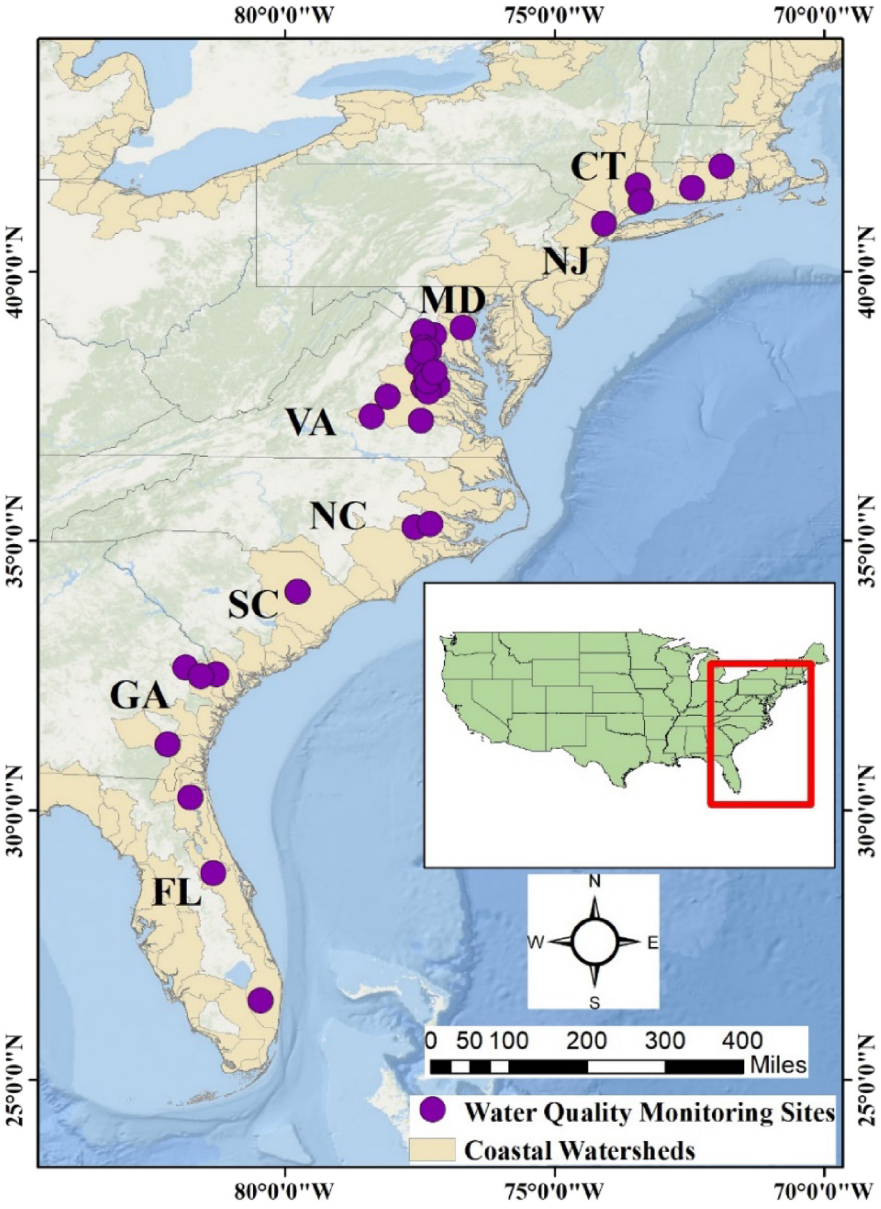

Fig. 1. Locations of 31 stream water quality stations across the U.S. Atlantic Coast.

incorporated diverse ecoregions ranging from the 'northeastern coastal zone' to the 'southern coastal plain'—representing gradients in climate, hydrology, land uses, soils, and geology (Omernik and Griffith, 2014; USGS, 2018). Drainage area of the monitoring sites ranged from approximately 1 to 25,443 km^2, whereas site-specific average stream flow varied from approximately 0.06 to 210 m^3/s (Table S3 in Supplementary materials). The corresponding land uses (see details in Text S1 of the Supplementary materials) represented varying amounts of agricultural land (approximately 0 to 92%), built-up land (4 to 87%), vegetated land (0 to 83%), wetland (0 to 46%), waterbody (0 to 5%), and open land (0 to 1%), draining into the stream monitoring locations.

Grab samples for the stream water quality variables and concurrent stream flow (Q) during 1998–2015 were obtained for the 31 streams from the National Water Quality Monitoring Council (NWQMC) database (NWQMC, 2017). The stream water quality dataset included DO, total phosphorus (TP), temperature of water (T_w), specific conductance, and pH. Salinity (S) was estimated from the specific conductance following Schemel (2001). The water quality data represented monthly to quarterly sampling frequencies across the stations and years, with samples collected at various hours (6:00 to 18:00), incorporating the productive phase of the 24-hour diel cycle. DO observations during the remaining nighttime hours (19:00 to 24:00 h) were not available for many of the stations. Further, data for TP, S, and pH during the 19:00 to 24:00 h of the diurnal cycles were in general not available.

Data for the stream top width (W) and depth (D) were not available in the NWQMC database. Concurrent (at the sampling time of water quality variables) data of W and D were estimated from their power law regression relationships with stream flow (Q) (r^2 = 0.53 to 0.96). The regression equations were estimated based on the available data from USGS (2017) (see details in Text S2 and Fig. S1 of the Supplementary materials). Concurrent atmospheric pressure (P_a) data were collected from the 4 × 4 km grid cells of National Solar Radiation Data Base (NSRDB) (NSRDB, 2017). Saturated concentration of dissolved oxygen (DO_{sat}) was estimated as a function of T_w, S, and P_a by using the nonlinear regression equations of the American Public Health Association (APHA; see Chapra, 2008).

The extreme outliers in data were detected and removed for each variable and site separately (see details in Table S1) by setting $P_{25} - 2 \times IQR$ and $P_{75} + 2 \times IQR$ as the lower and upper thresholds, respectively (Tukey, 1977); here P_{25} = 25th percentile, P_{75} = 75th percentiles, and IQR = interquartile range. The outliers were removed to avoid any biases

Table 1
Data summary of the water quality, climatic, and hydrologic variables during 1998–2015 in 31 streams located across the U.S. Atlantic Coast.

Variables	Mean	Standard deviation	Minimum	25th percentile	50th percentile	75th percentile	Maximum
P_a (mbar)	1009.8	8.7	976.9	1004.7	1010.4	1015.6	1035.4
T_w (°C)	15.4	8.0	0.1	8.5	15.6	22.2	32.3
TP (mg/l)	0.09	0.15	0.004	0.03	0.05	0.10	1.74
S (mg/l)	93.5	112.0	0.1	36.5	54.6	111.8	1219.9
pH	7.2	0.6	4.6	6.8	7.2	7.6	9.3
W (m)	55.23	52.02	0.81	20.14	36.55	68.11	200.30
D (m)	1.41	1.36	0.03	0.49	1.04	1.81	8.14
DO (mg/l)	9.3	2.4	1.6	7.5	9.1	11.2	16.0
DO_{sat} (mg/l)	10.2	1.8	7.3	8.6	9.9	11.7	14.7

Note: Sample size = 2429. P_a, T_w, TP, S, W, D, DO, and DO_{sat}, respectively, refer to atmospheric pressure, water temperature, total phosphorus, salinity, stream width, stream depth, dissolved oxygen, and saturated dissolved oxygen.

from unusually high or low values in our analyses and model estimation. The final dataset (sample size = 2429) was obtained by pooling data from all sites to incorporate wide ranges of water quality, climatic, and hydrologic conditions in the coastal streams (Table 1). The final dataset represented grab samples (and not their averages) of stream water quality variables (including DO) at monthly to quarterly sampling frequencies across the stream sites and the productive hours of diurnal cycles in various months of the year (Fig. S2 in the Supplementary materials).

2.2. Formulation of dimensionless numbers using Buckingham pi theorem

We formulated the dimensionless numbers using Buckingham pi theorem (Finnemore and Franzini, 2002; Kundu and Cohen, 2002) following the principle of dimensional homogeneity. Accordingly, if *n* dimensional variables have *r* fundamental dimensions, then the variables can be combined to form *n-r* dimensionless (i.e., pi or Π) numbers. The set of *n* variables (including stream DO) was determined by incorporating mechanistically relevant and important stream water quality variables and their drivers. Specific heat of water ($c_p = 4184\ J\ kg^{-1}\ °C^{-1}$) was incorporated to facilitate the formulation of dimensionless numbers involving T_w. Further, pH was converted to the concentration units of hydrogen ion (H). A functional relationship can be expressed by involving stream DO and the environmental drivers as follows:

$$f\left(DO, DO_{sat}, TP, H, S, W, D, P_a, T_w, c_p\right) = 0 \tag{1}$$

Here, the total number of variables, $n = 10$. Based on the units and dimensions of the variables (Table 2), the number of fundamental dimensions, $r = 4$ (mass: M; length: L; time: T; temperature: K). Therefore, six ($n\text{-}r = 6$) dimensionless (Π) numbers could be formulated and expressed in a functional form as follows:

$$\varphi(\Pi_1, \Pi_2, \Pi_3, \Pi_4, \Pi_5, \Pi_6) = 0 \tag{2}$$

Based on the pi theorem, four ($r = 4$) 'repeating variables' were selected in a way to involve all fundamental dimensions, without allowing formulation of dimensionless numbers among the repeating variables. A dimensionless number was then formulated by including one of the remaining variables with the repeating variables. For example, combining TP with the repeating variables of T_w, W, P_a, and c_p, the first pi number was formulated as follows:

$$\Pi_1 = T_w^a \cdot W^b \cdot P_a^c \cdot c_p^d \cdot TP \tag{3}$$

According to the principle of dimensional homogeneity:

$$M^0L^0T^0K^0 = (K)^a(L)^b\left(ML^{-1}T^{-2}\right)^c\left(L^2T^{-2}K^{-1}\right)^d\left(ML^{-3}\right) \tag{4}$$

Through simplification, we get the following expression:

$$M^0L^0T^0K^0 = M^{c+1}L^{b-c+2d-3}T^{-2c-2d}K^{a-d} \tag{5}$$

Equating the exponents of M, L, T, and K on both sides of Eq. (5), a system of equations can be obtained as follows:

$$c + 1 = 0 \tag{6}$$

$$b - c + 2d - 3 = 0 \tag{7}$$

$$-2c - 2d = 0 \tag{8}$$

$$a - d = 0 \tag{9}$$

The system of equations (Eqs. (6)–(9)) can be expressed in a matrix-vector format as follows:

$$\begin{bmatrix} 0 & 0 & 1 & 0 \\ 0 & 1 & -1 & 2 \\ 0 & 0 & -2 & -2 \\ 1 & 0 & 0 & -1 \end{bmatrix} \begin{bmatrix} a \\ b \\ c \\ d \end{bmatrix} = \begin{bmatrix} -1 \\ 3 \\ 0 \\ 0 \end{bmatrix} \tag{10}$$

Solving the system of equations, we get $a = 1, b = 0, c = -1$, and $d = 1$. This led to $\frac{c_p \cdot T_w \cdot TP}{P_a}$ as the first pi number (Π_1). However, any dimensionless number can be inversed for convenience of interpretations. For example, $\frac{c_p \cdot T_w \cdot TP}{P_a}$ was inverted to $\frac{P_a}{c_p \cdot T_w \cdot TP}$, which is the ratio of a positive driver (P_a) of stream DO to the negative drivers (T_w, TP). Π_1 was then expressed as follows:

$$\Pi_1 = \frac{P_a}{c_p \cdot T_w \cdot TP} \tag{11}$$

Table 2
Units and dimensions of variables involved in the dimensional analysis of stream DO.

Variables	Units	Dimensions
Dissolved oxygen (DO)	$kg\ m^{-3}$	$[ML^{-3}]$
Saturated concentration of dissolved oxygen (DO_{sat})	$kg\ m^{-3}$	$[ML^{-3}]$
Total phosphorus (TP)	$kg\ m^{-3}$	$[ML^{-3}]$
Hydrogen ion (H)	$kg\ m^{-3}$	$[ML^{-3}]$
Salinity (S)	$kg\ m^{-3}$	$[ML^{-3}]$
Stream width (W)	m	[L]
Stream depth (D)	m	[L]
Atmospheric pressure (P_a)	$kg\ m^{-1}\ s^{-2}$	$[ML^{-1}\ T^{-2}]$
Stream water temperature (T_w)	°C	[K]
Specific heat of water (c_p)	$J\ kg^{-1}\ °C^{-1}$	$[L^2\ T^{-2}\ K^{-1}]$

Similarly, Π_2 to Π_6 for the chosen set of repeating variables were formulated as follows:

$$\Pi_2 = \frac{P_a}{c_p \cdot T_w \cdot H}$$

$$\Pi_3 = \frac{P_a}{c_p \cdot T_w \cdot S}$$

$$\Pi_4 = \frac{P_a}{c_p \cdot T_w \cdot DO}$$

$$\Pi_5 = \frac{P_a}{c_p \cdot T_w \cdot DO_{sat}}$$

$$\Pi_6 = \frac{W}{D}$$

The Π_4 and Π_5 were combined to form the dimensionless DO number as follows:

$$\frac{\Pi_5}{\Pi_4} = \frac{P_a}{c_p \cdot T_w \cdot DO_{sat}} \div \frac{P_a}{c_p \cdot T_w \cdot DO} = \frac{DO}{DO_{sat}} \tag{12}$$

The derived set of five dimensionless numbers was expressed in functional form as follows:

$$\varphi\left(\frac{DO}{DO_{sat}}, \frac{P_a}{c_p \cdot T_w \cdot TP}, \frac{P_a}{c_p \cdot T_w \cdot H}, \frac{P_a}{c_p \cdot T_w \cdot S}, \frac{W}{D}\right) = 0 \tag{13}$$

Various sets of dimensionless numbers were formulated by iteratively changing the 'repeating variables' (see Table S7 in Supplementary materials). However, the derived numbers from different iterations could be combined to obtain the mechanistically meaningful set of five dimensionless numbers (Eq. (13)). The dimensionless DO number, $\frac{DO}{DO_{sat}}$ represented the fraction of in-stream DO saturation value, and was termed the 'DO saturation' number. The other four dimensionless numbers represented the interactive controls of various climatic, hydrologic, biochemical, and ecological drivers on stream DO. However, each of the remaining numbers represented a ratio of a positive driver (P_a, W) to the negative drivers and correlates (T_w, TP, S, D, H) of stream DO. To reflect these interactive ratio of positive control (i.e., source) to the overall negative control (i.e., sink) of stream DO, the four dimensionless numbers were combined together (by multiplications) in the following form for further analyses:

$$\frac{P_a}{c_p \cdot T_w \cdot TP} \times \frac{P_a}{c_p \cdot T_w \cdot H} \times \frac{P_a}{c_p \cdot T_w \cdot S} \times \frac{W}{D} = \frac{P_a^3 \cdot W}{c_p^3 \cdot T_w^3 \cdot TP \cdot H \cdot S \cdot D} \tag{14}$$

The new dimensionless number, $\frac{P_a^3 \cdot W}{c_p^3 \cdot T_w^3 \cdot TP \cdot H \cdot S \cdot D}$ was termed the stream 'metabolic' number, which represented the contrasting (sources versus sinks) as well as the collective (overall interactive) controls of the major environmental drivers on stream metabolism (Bernhardt et al., 2018). The remarkable parametric reduction of 10 original variables to only two dimensionless groups ('DO saturation' and 'metabolic' numbers) was defined as the stream 'biogeochemical similitude' in this study. Based on the pi theorem, the 'DO saturation' number was expressed as a function (ψ) of the 'metabolic' number as follows:

$$\frac{DO}{DO_{sat}} = \psi\left(\frac{P_a^3 \cdot W}{c_p^3 \cdot T_w^3 \cdot TP \cdot H \cdot S \cdot D}\right) \tag{15}$$

2.3. Investigation of emergent pattern and environmental regimes

We scatter-plotted the 'DO saturation' number (on the vertical axis) with the 'metabolic' number (on the horizontal axis) to identify any apparent emergent pattern between the two dimensionless numbers. The emergence would be indicated by a potential collapse of observational data from diverse streams across the U.S. Atlantic Coast on a generalized characteristic curve or process diagram. The generalized diagram could indicate environmental regimes of stream metabolism, with mechanistically meaningful thresholds for separation and transition among the regimes. Any boundaries (e.g., breakpoints) between the metabolic regimes were determined by visually apparent points of inflection on the generalized characteristic process diagram. These boundaries were further corroborated by identifying mechanistically meaningful thresholds of the environmental drivers (i.e., original variables) near the breakpoints. Further, the null hypothesis of no significant difference in DO and the environmental drivers among the potential metabolic regimes were tested at the 95% confidence level with ANOVA for linear mixed-effects models. This method of ANOVA was chosen based on the possibility of repeated measures of variables in time from stream sites across the environmental regimes. We applied the 'residual' method for computing degrees of freedom with the F-test. All variables were examined for approximate normality and log10-transformed, as necessary (see Figs. S3 and S4 in Supplementary materials), for the ANOVA analysis. The analysis was performed in MATLAB version R2020b.

2.4. Development of scaling relationship

The potential scaling of 'DO saturation' number with the 'metabolic' number was investigated as an emergent power law function as follows:

$$Y = 1 - \alpha X^{\beta} \tag{16}$$

where $Y = \frac{DO}{DO_{sat}}$, $X = \frac{P_a^3 \cdot W}{c_p^3 \cdot T_w^3 \cdot TP \cdot H \cdot S \cdot D}$, α is the location parameter, and β is scaling exponent (i.e., shape parameter). The emergent scaling model (Eq. (16)) was estimated with the observed data (binned-averaged data if a large scatter was apparent in the original data) from streams across the U.S. Atlantic Coast by using the Levenberg-Marquardt non-linear least squares algorithm. The prediction efficiency and accuracy of the scaling model were measured, respectively, by the Nash-Sutcliffe Efficiency (NSE) and the ratio of root-mean-square-error to the standard deviation of observations (RSR). NSE = 1.0 and RSR = 0 indicate a perfectly predictive model (Moriasi et al., 2007; see Text S3 in Supplementary materials).

The model parameters (α, β) were robustly estimated by performing cross-validations (80% data for calibration and 20% data for validation) with a bootstrap Monte-Carlo resampling of the dataset 1000 times. The final estimates of individual parameters and model performance metrics (NSE, RSR) were obtained by averaging the corresponding 1000 estimations. The model exponent (β) indicated the potential scaling relationship between the response and predictor dimensionless numbers. Standard deviation and coefficient of variation (CV) of the parameters were also computed to indicate the associated uncertainties in the estimation process. The estimated scaling relationship was then rearranged by bringing DO_{sat} on the right-hand-side of Eq. (16) to develop a generalized nonlinear model for predicting DO in diverse streams across the U.S. Atlantic Coast.

3. Results

3.1. Emergent pattern and metabolic regimes

A semi-logarithmic plot of 'DO saturation' number $\left(\frac{DO}{DO_{sat}}\right)$ with the 'metabolic' number $\left(\frac{P_a^3 \cdot W}{C_p^3 \cdot TW^3 \cdot TP \cdot H \cdot Sal \cdot D}\right)$ led to collapse of observations from various coastal streams into a unique dimensionless curve—suggesting an emergent process diagram (Fig. 2a). Given the scatter in the original data, observations of the 'metabolic' number were binned and averaged for

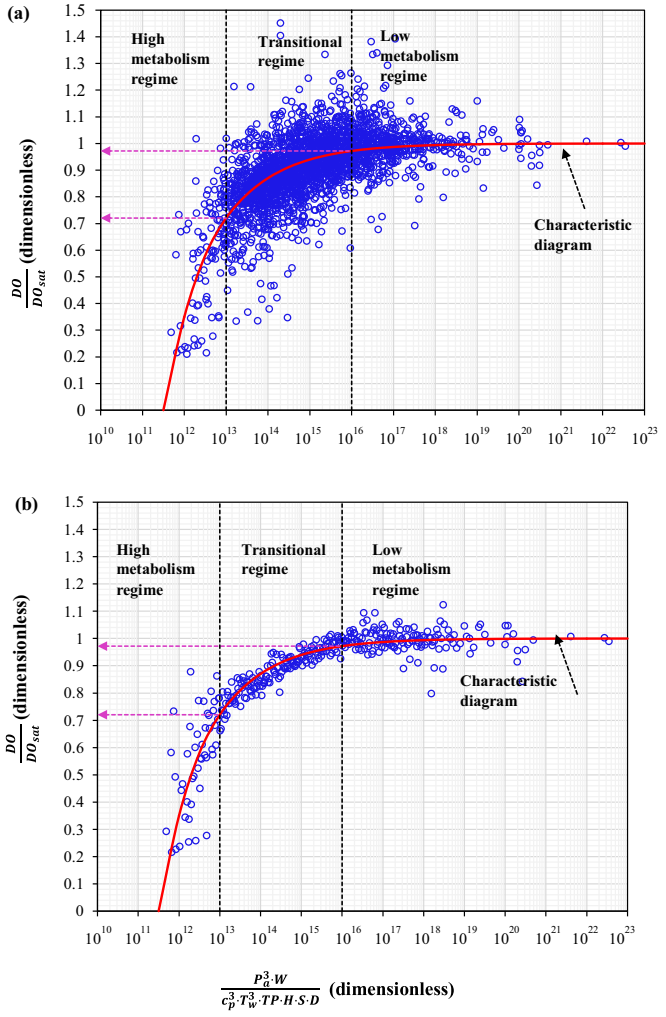

Fig. 2. Plot of the 'DO saturation' number $\left(\frac{DO}{DO_{sat}}\right)$ with the 'metabolic' number $\left(\frac{P_a^3 \cdot W}{c_p^3 \cdot T_w^3 \cdot TP \cdot H \cdot S \cdot D}\right)$ with the (a) original data (sample size = 2429) and (b) bin-averaged data (sample size = 341), indicating collapse of observations from diverse coastal streams on a generalized characteristic process diagram. Original observations of the 'metabolic' number were binned and averaged for each $log_{10}\left(\frac{P_a^3 \cdot W}{c_p^3 \cdot T_w^3 \cdot TP \cdot H \cdot S \cdot D}\right) = 0.02$, and plotted with the corresponding averages of $\frac{DO}{DO_{sat}}$. The solid red lines indicate the conceptual characteristic process diagram. The hashed (vertical) black lines separate the three regimes. The hashed (horizontal) magenta arrows indicate the thresholds of $\frac{DO}{DO_{sat}}$ in regime transitions.

each $log_{10}\left(\frac{P_a^3 \cdot W}{c_p^3 \cdot T_w^3 \cdot TP \cdot H \cdot S \cdot D}\right) = 0.02$, and plotted with the corresponding averages of $\frac{DO}{DO_{sat}}$ (Fig. 2b).

The 'DO saturation' number nonlinearly increased with the increasing 'metabolic' number up to the vicinity of complete saturation, and then turned into a nearly horizontal line. Visually apparent points of inflection on the generalized characteristic process diagram indicated two contrasting environmental regimes separated by a 'transitional' regime (Fig. 2a, b). When the stream 'metabolic' number $\geq 10^{16}$ on the characteristic diagram, DO remained close to full saturation (e.g., $\frac{DO}{DO_{sat}} \geq 0.97$)—indicating an environmental regime with a low rate of metabolic consumption of DO. This stream environmental condition was termed the 'low metabolism' regime. In contrast, 'metabolic' number $\leq 10^{13}$ represented an environmental regime where the 'DO saturation' was relatively low ($\frac{DO}{DO_{sat}} \leq 0.72$) and dropped at a faster rate with the decreasing 'metabolic' number. This regime indicated a highly favorable environmental condition for metabolic consumption of DO, and was termed the 'high metabolism' regime. The two regimes were connected by a 'transitional' regime (10^{13} < 'metabolic' number < 10^{16}, and 0.72 < 'DO saturation' number < 0.97), where the 'DO saturation' gradually decreased with the decrease of 'metabolic' number, transforming the stream condition from low to high metabolism regime.

3.2. Comparison of regime-specific stream DO and the environmental drivers

The differences in DO and the environmental drivers among the three metabolic regimes were apparent from the results of ANOVA for linear mixed-effects model (Tables S8, S9, and S10). The hypothesis of no significant difference in DO was rejected between the 'high metabolism' and the 'low metabolism' regimes ($F_{1,672} = 453.33$, p value < 0.001), between the 'high metabolism' and the 'transitional' regimes ($F_{1,1860} = 172.59$, p value < 0.001), and between the 'transitional' and the 'low metabolism' regimes ($F_{1,2320} = 1333.60$, p value < 0.001). Stream TP, T_w, pH, W, P_a, and DO_{sat} were also significantly different between and among the regimes ($F_{1,672\ to\ 2320} = 4.27$ to 1433.20, p value < 0.05). Further, there were significant differences in S ($F_{1,672\ to\ 1860} = 6.7$ to 35.48, p value < 0.01) and in D ($F_{1,672\ to\ 1860} = 8.3$ to 11.3, p value < 0.01) between the 'high metabolism' and 'low metabolism' regimes, as well as between the 'high metabolism' and 'transitional' regimes. However, S ($F_{1,2320} = 0.002$, p value = 0.97) and D ($F_{1,2320} = 3$, p value = 0.08) were not significantly different between the 'transitional' and 'low metabolism' regimes.

The characteristic differences of the three metabolic regimes were demonstrated in the regime-specific original (unsmoothed) data summary of DO and the environmental drivers (Table 3; Fig. S5 in Supplementary materials). The 'low metabolism' regime was characterized by relatively low stream temperature (mean T_w = 7.4 °C), low nutrient (mean TP = 0.04 mg/l), high DO (mean = 12.1 mg/l), and high DO_{sat} (mean = 12.2 mg/l). Conversely, the 'high metabolism' regime corresponded to high values of stream temperature (mean T_w = 25 °C) and nutrient (mean TP = 0.31 mg/l), and substantially lower values of DO (mean = 5.2 mg/l) and DO_{sat} (mean = 8.3 mg/l). Further, the 'high metabolism' regime corresponded to relatively lower values of stream width (mean W = 46.65 m) and pH (mean = 6.7) than that of the 'low metabolism' regime (mean W = 73.51 m, and mean pH = 7.5). The 'high metabolism' regime was also characterized by higher values of stream depth (mean D = 2.83 m) and salinity (mean S = 227 mg/l) than the 'low metabolism' regime (mean D = 1.17 m, mean S = 72.5 mg/l). In contrast, the 'transitional' regime had intermediate values of DO (mean = 8.7 mg/l), DO_{sat} (mean = 9.7 mg/l), and the environmental drivers (e.g., mean T_w = 17.4 °C, mean TP = 0.10 mg/l, mean S = 92.10 mg/l, mean pH = 7.1, mean D = 1.4 m, mean W = 49.85 m).

3.3. Emergent scaling relationship

Given the large scatter in the original data (Fig. 2a), we estimated the proposed scaling relationship (Eq. (16)) of the 'DO saturation' number as a function of the 'metabolic' number based on the binned-average data (Fig. 2b) as follows:

$$\frac{DO}{DO_{sat}} = 1 - 6024.04\left(\frac{P_a^3 \cdot W}{c_p^3 \cdot T_w^3 \cdot TP \cdot H \cdot S \cdot D}\right)^{-\frac{1}{3}} \quad (17)$$

The model (Eq. (17)) efficiency and accuracy from bootstrap Monte-Carlo resampling suggested very good prediction performance (Moriasi et al., 2007) in both training (i.e., calibration; NSE = 0.85 and RSR = 0.39) and validation (NSE = 0.83 and RSR = 0.40). We presented the observed versus predicted 'DO saturation' number plot and the associated residual plot based on all binned-average data without resampling (Fig. 3a, b). The model parameters, scale factor (α = 6024.04, p value < 0.01) and exponent ($\beta = -\frac{1}{3}$, p value < 0.01), were significant at the 95% confidence level. The standard deviations (and coefficients of variation) of the scale factor and exponent were 279.63 (5%) and 0.02 (6%), respectively. The relatively small standard deviations and coefficients of variation emphasized the stability and low

Table 3
Data summary of the stream water quality variables and their drivers during 1998–2015 in the 'low metabolism', 'transitional', and 'high metabolism' regimes, as shown in Fig. 2.

Variables	Mean	Standard deviation	Minimum	25th percentile	50th percentile	75th percentile	Maximum
'Low metabolism' regime							
P_a (mbar)	1010.3	9.3	976.9	1004.9	1010.6	1016.6	1035.4
T_w (°C)	7.4	6.2	0.1	3.3	5.6	9.8	30.7
TP (mg/l)	0.04	0.04	0.004	0.02	0.03	0.04	0.40
S (mg/l)	72.5	51.2	0.1	37.9	51.8	97.1	467.7
pH	7.5	0.6	5.8	7.1	7.5	7.9	9.1
W (m)	73.51	64.07	2.28	24.93	49.72	118.32	198.63
D (m)	1.17	0.78	0.07	0.54	1.07	1.66	4.34
DO (mg/l)	12.1	1.6	6.9	11.3	12.3	13.1	16.0
DO_{sat} (mg/l)	12.2	1.6	7.4	11.3	12.5	13.3	14.7
'Transitional' regime							
P_a (mbar)	1009.6	8.6	980.4	1004.4	1010.3	1015.5	1031.5
T_w (°C)	17.4	6.8	1.9	11.8	17.6	22.8	32.3
TP (mg/l)	0.10	0.13	0.01	0.04	0.06	0.11	1.56
S (mg/l)	92.1	110.3	12.1	35.5	55.1	114.1	1219.9
pH	7.1	0.6	5.3	6.8	7.1	7.5	9.3
W (m)	49.85	46.77	0.92	19.36	33.33	62.96	200.30
D (m)	1.40	1.35	0.04	0.47	1.02	1.86	8.14
DO (mg/l)	8.7	1.8	2.9	7.4	8.6	10.0	14.4
DO_{sat} (mg/l)	9.7	1.4	7.3	8.5	9.5	10.8	13.9
'High metabolism' regime							
P_a (mbar)	1011.6	5.4	996.2	1009.2	1011.7	1015.5	1026.0
T_w (°C)	25.0	3.8	12.8	22.0	26.2	28.0	32.0
TP (mg/l)	0.31	0.39	0.03	0.10	0.14	0.24	1.74
S (mg/l)	227.0	226.6	12.1	40.9	82.4	428.8	745.8
pH	6.7	0.8	4.6	6.1	6.5	7.4	8.0
W (m)	46.65	39.14	0.81	21.07	34.06	60.93	162.52
D (m)	2.83	2.61	0.03	0.54	1.68	5.24	7.41
DO (mg/l)	5.2	1.8	1.6	4.1	5.5	6.5	9.1
DO_{sat} (mg/l)	8.3	0.6	7.3	7.8	8.1	8.7	10.7

Note: P_a, T_w, TP, S, W, D, DO, and DO_{sat}, respectively, refer to atmospheric pressure, water temperature, total phosphorus, salinity, stream width, stream depth, dissolved oxygen, and saturated dissolved oxygen.

uncertainty in the scaling parameters. The model exponent ($\beta = -\frac{1}{3}$) indicated an emergent power law scaling relationship of 'DO saturation' number with the 'metabolic' number across diverse coastal streams.

The developed equation between the dimensionless numbers (Eq. (17)) was further rearranged by bringing DO_{sat} on the right-hand-side and expressed as a generalized predictive model of DO for diverse streams across the U.S. Atlantic Coast as follows:

$$DO = DO_{sat}\left[1 - 6024.04\left(\frac{P_a^3 \cdot W}{c_p^3 \cdot T_w^3 \cdot TP \cdot H \cdot S \cdot D}\right)^{-\frac{1}{3}}\right] \quad (18)$$

The model (Eq. (18)) was used to predict DO in streams of the U.S. Atlantic Coast and compared with all the original (i.e., unbinned) data. Notwithstanding the visible over- and under-predictions, the efficiency and accuracy (NSE = 0.83 and RSR = 0.41; Fig. 4a, b) of the similitude-based power law model demonstrated very good performance in predictions of DO (Moriasi et al., 2007). This indicated the substantial generality (i.e., robustness) of the model to predict DO in diverse streams and metabolic regimes across the Atlantic Coast of USA. The state-specific color codes on the observed versus predicted DO and the associated residual plots (Fig. 4a, b) showed that the over- and under-predictions of DO were distributed in the streams across the states.

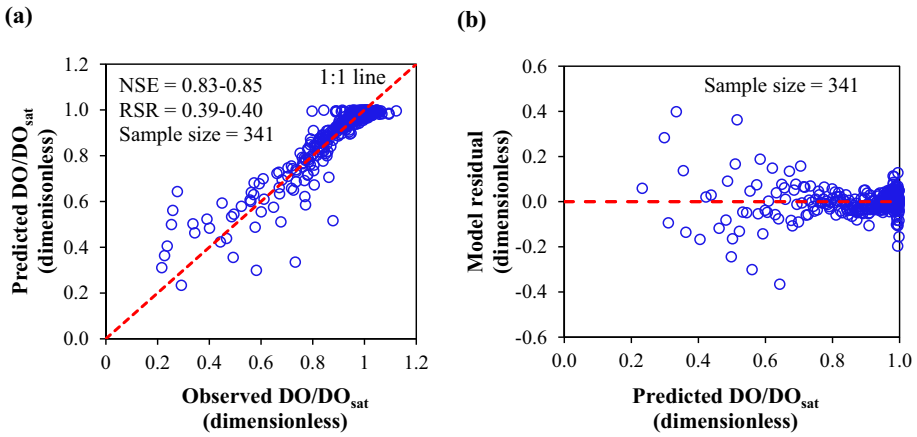

Fig. 3. Plots of predicted 'DO saturation' number (DO/DO_{sat}) with (a) the smoothed (binned-average) observations and (b) the corresponding model residuals during 1998–2015 for streams across the U.S. Atlantic Coast.

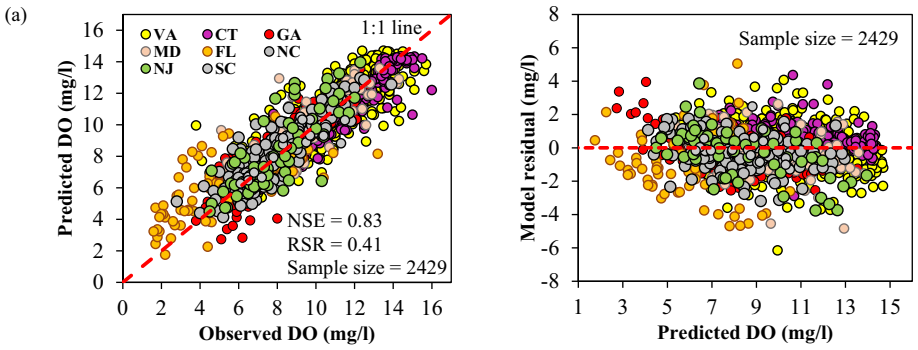

Fig. 4. Plots of predicted DO with (a) the original (i.e., unsmoothed/unbinned) observations and (b) the corresponding model residuals during 1998–2015 for streams across the U.S. Atlantic Coast. The plots have been color-coded by states.

4. Discussion

4.1. Stream biogeochemical similitude and emergent scaling law

The research involved stream DO and the environmental drivers within a dimensional analysis framework, and unraveled a remarkable stream 'biogeochemical similitude' (reductions of 10 original variables into two dimensionless numbers) and functional convergence. The unique curve of the 'DO saturation' number $\left(\frac{DO}{DO_{sat}}\right)$ with the 'metabolic' number $\left(\frac{P_a^3 \cdot W}{c_p^3 \cdot T_w^3 \cdot TP \cdot H \cdot S \cdot D}\right)$ indicated a collapse of data from diverse coastal stream ecosystems on an emergent characteristic process diagram. The 'metabolic' number included the drivers of DO sources (e.g., reaeration, atmospheric diffusion) in the numerator and sinks (organic decomposition, respiration, and nitrification) in the denominator. It represented the contrasting (sources versus sinks) as well as the collective (overall interactive) controls of various environmental drivers on stream DO. The developed scaling relationship of 'DO saturation' number as a function of the 'metabolic' number (with an exponent of $\frac{1}{3}$) indicated the emergence of interactive processes and the underlying organizing principles of metabolism in coastal streams. This emergence of processes, in turn, led to the generalized scaling law and robust empirical model (Eq. (18)) to predict (NSE = 0.83 and RSR = 0.41) stream DO in diverse streams located across the U.S. Atlantic Coast.

4.2. Stream metabolism regimes and the characteristics of environmental drivers

Stream metabolism is directly linked with stream DO, and any variation in the pattern of stream DO reflects the variation in the rates of gross primary production (GPP), ecosystem respiration (ER), and reaeration (Bernhardt et al., 2018). In the existing literature, stream metabolism has been referred to any characteristic temporal patterns of DO, GPP, and ER in response to the stream stressors (Bernhardt et al., 2018; Koenig et al., 2019; Savoy et al., 2019). For example, Bernhardt et al. (2018) identified river metabolism regimes based on the temporal patterns of DO (% saturation) and GPP for four rivers from the contrasting U.S. states of Wisconsin, Alabama, Texas, and Oregon. Accordingly, in our study, the term 'metabolism regime' has been defined based on any mechanistically meaningful transition on the characteristic process diagram of the 'DO saturation' number $\left(\frac{DO}{DO_{sat}}\right)$ in response to the stream biogeochemical processes.

A novel contribution of our study is the achievement of stream 'biogeochemical similitude', which resulted in a remarkable parametric reduction of 10 original ecosystem variables to only two dimensionless groups ('DO saturation' and 'metabolic' numbers). The similitude inherently contributes to the reduction of uncertainty and equifinality in estimating a predictive model of stream DO using the two dimensionless numbers. However, it is worth mentioning here that equifinality is a classical issue mainly for a parameter-rich process-based model (Beven and Binley, 1992; Beven and Freer, 2001; Arsenault and Brissette, 2014). In contrast, our scaling-based empirical model used only one dimensionless variable ('metabolic' number) to predict the response ('DO saturation'), involving two parameters (α, β) that were robustly estimated with low uncertainty (coefficient of variation = 5 to 6%).

Another unique contribution of our study is that we classified the metabolism regimes in terms of the dimensionless 'metabolic' number, which synthesizes the interactions of major hydroclimatic and biochemical drivers of stream DO. The characteristic process diagram suggested low, transitional, and high stream metabolism regimes, which had distinct environmental characteristics (Table 3). Apart from the occasional exceptions for S and D, stream DO and the corresponding environmental drivers were significantly different among the three metabolism regimes. Overall, the negative and positive drivers of stream DO tended to increase, respectively, from low to high and high to low metabolism regimes. Furthermore, being dimensionless, the 'metabolic' number led to a scale-invariant and generalized classification of stream metabolism—which is apparent from the collapse of diverse stream ecosystems on the emergent characteristic process diagram (Fig. 2a, b). This significantly contributes to fill in the existing knowledge-gaps and resolves the barrier of variable biogeochemical controls on stream DO to develop a generalized understanding, scaling relationship, and predictive model for diverse coastal streams across a large spatial scale.

The substantially different values of the negative drivers likely resulted in the contrasting stream DO concentrations among the three metabolism regimes. The lower DO concentrations (mean = 5.2 mg/l) in the 'high metabolism' regime were largely caused by the warmer stream temperature (mean = 25 °C) and higher concentrations of total phosphorus (mean = 0.31 mg/l). This combination of temperature and nutrient presumably provided a favorable environment for algal bloom (Dodds and Smith, 2016) and a subsequent higher decomposition of organic matter and nitrification—leading to a stronger microbial consumption of DO (Schaefer and Hollibaugh, 2017; Poikane et al., 2021). Stream DO in the 'high metabolism' regime was also substantially impacted by the reduced solubility of oxygen in water due to the high temperatures (Chapra, 2008; Ni et al., 2019). In contrast, the higher DO concentrations in the 'low metabolism' regime were mainly caused by the cooler stream temperature and lower concentrations of total phosphorus. These combinations apparently led to a higher oxygen solubility in stream water, apart from the unfavorable environmental condition for microbial consumption of stream DO. The moderate level of dissolution and microbial consumption, driven by the intermediate (i.e., in-between high and low metabolism) stream temperature and total phosphorus, resulted in the intermediate DO concentrations for the 'transitional' regime.

Relative variations of other drivers among the three regimes also contributed to their contrasting DO concentrations (Table 3). For example, the lower stream DO of the 'high metabolism' regime may also partly be attributed to its higher salinity (mean = 227 mg/l), which contributed

electrolytes and resulted in a reduced oxygen solubility in stream water (Garcia and Gordon, 1992; Chapra, 2008). However, lower values of both pH and DO in the 'high metabolism' regime than that of the other regimes (Table 3) suggested a positive interrelation of DO and pH, which may be attributed to the increased organic matter and microbial decomposition due to the elevated stream temperature and total phosphorus. Higher microbial decomposition concurrently reduces DO and pH by consuming oxygen and producing carbon dioxide, leading to an increase in stream acidity (Romeijn et al., 2019). The reaeration potential was high in the 'low metabolism' regime due to the higher stream width to depth ratio (mean $\frac{W}{D}$ ≈62.83), which likely contributed to the elevated stream DO (van Dael et al., 2020; Bennett and Rathbun, 1972). The higher $\frac{W}{D}$ ratio also increased stream exposure to photosynthetically active radiation to boost DO through photosynthesis (Hondzo et al., 2013; Zhi et al., 2021). In contrast, the lower DO in the 'high metabolism' regime might be further impacted by the low reaeration potential due to a lower width to depth ratio (mean $\frac{W}{D}$ ≈16.48). The effect of stream geometry was further corroborated by an intermediate reaeration potential (mean $\frac{W}{D}$ ≈35.61) and DO concentrations in the 'transitional' regime. Notably, the mean $\frac{W}{D}$ of the 'low metabolism' regime was 1.76 (~2) times higher than that of the 'transitional' regime, whereas the mean $\frac{W}{D}$ of the 'transitional' regime was 2.16 (~2) times higher than that of the 'high metabolism' regime.

4.3. Critical environmental thresholds separating the metabolism regimes

The critical threshold separating the 'low metabolism' and the 'transitional' regimes was 10^{16} for the 'metabolic' number and 0.97 for the 'DO saturation' number (Fig. 2a, b). In contrast, a 'metabolic' number of 10^{13} and 'DO saturation' number of 0.72 separated the 'transitional' and 'high metabolism' regimes. Given the scatter in the original data (Fig. 2a), we explored possible boundary values of stream DO and the environmental drivers among the three metabolism regimes based on the respective quartiles (i.e., pseudo-thresholds) of the original variables. For example, the lower quartile (25th percentile) of DO in the 'low metabolism' regime (11.3 mg/l) was close to the upper quartile (75th percentile) of DO in the 'transitional' regime (10 mg/l). The average of the two values (DO ≈ 11 mg/l) could be considered a pseudo-threshold between the two regimes. However, the upper quartile of total phosphorus in the 'low metabolism' was 0.04 mg/l, which also represented the lower quartile of total phosphorus in the 'transitional' regimes (Table 3). Further, the upper and lower quartiles of stream temperature, respectively, in the 'low metabolism' and 'transitional' regimes, were ~9.8 °C and 11.8 °C (average ≈ 11 °C). Therefore, 0.04 mg/l, and 11 °C could be considered as the pseudo-thresholds of total phosphorus and water temperature, separating the 'low metabolism' and 'transitional' regimes. Similarly, the pseudo-thresholds of DO, total phosphorus, and water temperature between the 'transitional' and 'high metabolism' regimes were, respectively, ~7 mg/l, ~0.10 mg/l, and ~22 °C (Table 3).

No boundary values (thresholds) were found in the other environmental drivers (S, pH, P_a, W, D), although these drivers were overall (with some exceptions for S and D) significantly different among the three stream metabolism regimes. It is worth stating here that majority of the environmental drivers were not strongly correlated, as apparent in the regime-specific correlation matrices (see Table S11 in Supplementary materials). The absence of thresholds in the other drivers reemphasized the scope and usefulness of the stream 'biogeochemical' similitude and dimensionless numbers. Nevertheless, we posit that a stream ecosystem would likely be in the 'high metabolism' regime if $T_w \geq 22$ °C, TP ≥ 0.10 mg/l, and DO ≤ 7 mg/l. In contrast, a stream ecosystem would represent a 'low metabolism' regime when $T_w \leq 11$ °C, TP ≤ 0.04 mg/l, and DO ≥ 11 mg/l. Otherwise, the stream metabolism would represent a 'transitional' regime (i.e., 11 °C < T_w < 22 °C, 0.04 mg/l < TP < 0.10 mg/l, and 7 mg/l < DO < 11 mg/l). However, the quartile-based pseudo-thresholds of T_w, TP, and DO did not include 25% data in each regime. The pseudo-thresholds may still be used to classify a stream regime if the outcome is consistent with that obtained by using the thresholds of the 'metabolic' and 'DO saturation' numbers.

The pseudo-thresholds of total phosphorus (~0.04 and ~0.10 mg/l) and stream temperature (~11 and ~22 °C) among the three regimes were comparable to their limiting thresholds reported in literature. For instance, Poikane et al. (2021) reported a multitude of studies that investigated the effect of nutrients on stream ecology. Majority of the studies found excessive stream algal growth when total phosphorus exceeded the threshold between 0.03 and 0.06 mg/l, which was comparable to 0.04 mg/l in our study. Further, the identified threshold of ~0.10 mg/l for total phosphorus was equal to the total phosphorus limit recommended by the U.S. EPA to control eutrophication in flowing waters (USEPA, 1986; Wang et al., 2015; Jalali and Jalali, 2017). Efficiency for majority of the organic waste decomposing microorganisms (e.g., mesophilic and thermophilic bacteria, fungi) is substantially decreased below ~10 °C temperature (Ferreira and Chauvet, 2011; Keenleyside, 2019), which was comparable to the identified threshold of ~11 °C for stream temperature in our study. Further, our identified threshold of 22 °C corresponded to the optimum temperature range (20 to 35 °C) for microbially mediated reactions in aquatic ecosystems (Kadlec and Reddy, 2001; Yuan et al., 2019).

4.4. Variation of stream metabolism

The seasonal variation of the site-specific 'metabolic' numbers across the year (Fig. 5) indicated a dynamic nature of stream metabolism, leading to the transition of a stream site from low to transitional and from transitional to high metabolism regime. The metabolic number was lower in the warm season (May–October) than that of the cold season (November–April) across all the stream sites (Yu et al., 2016; Martinez-Villalobos and Neelin, 2018). Further, majority of the northern (e.g., CT) sites had a higher metabolic number than the southern (e.g., FL) sites, regardless of seasons. These suggested strong effects of T_w to control stream metabolism, leading to a lower metabolic number during the occurrence of warmer stream temperatures. Further, the temporal distribution of the metabolic number varied across the stream sites, as the sites incorporated wide ranges of climatic, hydrologic, and biogeochemical conditions (Table S2)—leading to differing controls from the hydroclimatic and biochemical drivers. Between the warm and cold seasons, the metabolic number varied mostly from low to transitional metabolism regime in the southern sites and from transitional to high metabolism regime in the northern sites. The lower metabolic number of the southern sites (Fig. 5) than the northern sites might be caused by the combined effects of higher T_w and TP in the southern sites (Table S2). This reiterated that the metabolism status of a stream might change in time (e.g., season) based on the prevailing environmental conditions. However, an important caveat of our study is that our findings are mainly based on the analyses of data collected during the productive phase (6 to 18 h) of the diurnal cycles. Subject to the availability of diel (24 h) data for DO and the environmental drivers across a large spatial gradient, future research should investigate the dynamics of stream DO and metabolism status across the diel hours based on the characteristic process diagram and scaling relationship.

4.5. Implications for water resources management

The emergent similitude, scaling relationship, and predictive model of stream DO are expected to aid in achieving healthy water quality in diverse coastal streams. The 'metabolic' number and the generalized scaling relationship can help water managers determine the dynamic response of stream water quality and ecosystem health under a changing climate, land uses, and sea level rise. For example, the 'metabolic' number and environmental regimes can be employed to study how a stream dynamically changes its metabolism (e.g., Table S12) due to the changes in climate, stream biogeochemistry, and saltwater intrusion—with or without alterations in stream geometric properties (i.e., width and depth).

The scaling model would also guide the water managers on how the stream water quality drivers (e.g., temperature, nutrient, salinity, and

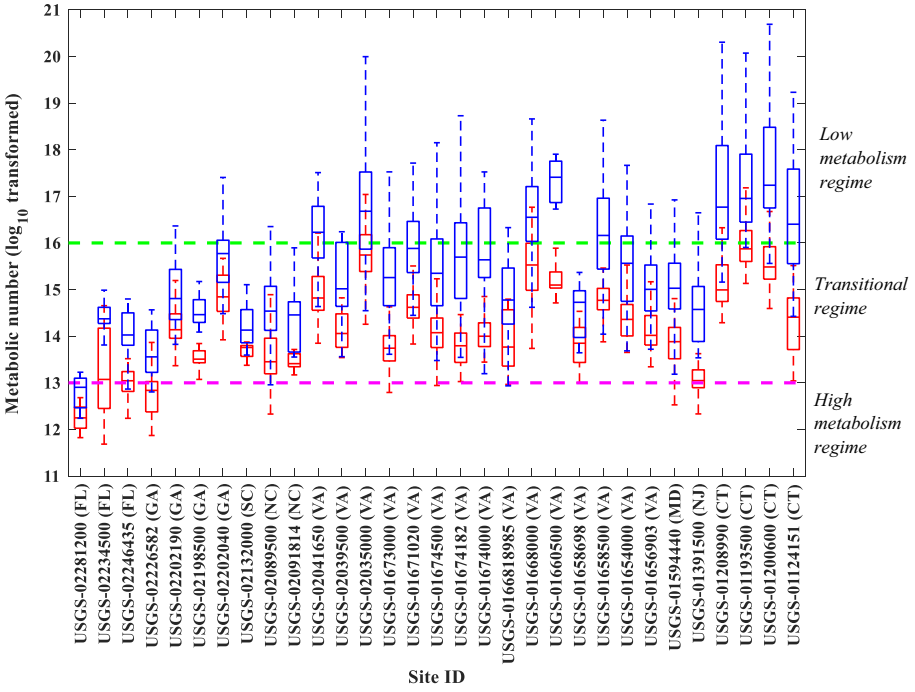

Fig. 5. Boxplots showing the variation of the 'metabolic' number in warm season (May–October; red boxes and whiskers) and cold season (November–April; blue boxes and whiskers) during 1998–2015 for various stream sites located across the U.S. Atlantic Coast. The parentheses alongside the site ID refers to the respective U.S. states. The sites have been stated according to increasing northern latitude from left to right; the most southern site is stated at the left and the most northern site is stated at the right. The hashed green and purple lines separate the three (low, transitional, and high metabolism) regimes.

channel geometry) should be managed to recover a stream from low to high level of DO—facilitating stream restoration. It would enhance their capability in selecting the most optimum combination of controlling measures to restore a hypoxic stream, either by increasing the assimilative capacity of the stream (e.g., altering channel geometry to increase reaeration) or by reducing pollutant loads. Unlike a locally developed stream water quality model, the scaling-based generalized model is able to predict DO in diverse streams across the U.S. Atlantic Coast. This can guide a cost-benefit analysis of alternative strategies for an efficient management of coastal stream ecosystems.

5. Conclusions

We investigated the emergent 'biogeochemical' similitude (parametric reduction), characteristic process diagram, and generalized metabolic scaling of DO in coastal streams across a large spatiotemporal scale of the U.S. Atlantic Coast by employing dimensional analysis. Two mechanistically meaningful dimensionless numbers were found as the stream 'metabolic' number and the fraction of 'DO saturation' number. The 'metabolic' number represented the contrasting (sources versus sinks) as well as synergistic control on stream DO from various hydroclimatic and biochemical drivers. The dimensionless numbers led to the development of an emergent process diagram, indicating three metabolism regimes (high, transitional, and low). The 'low metabolism' regime was represented by the critical thresholds of 10^{16} (or higher) for the 'metabolic' number and 0.97 (or higher) for the 'DO saturation' number. In contrast, the 'high metabolism' regime corresponded to the critical 'metabolic' number of 10^{13} (or lower) and critical 'DO saturation' number of 0.72 (or lower). The coastal streams represented a 'transitional' metabolism regime otherwise (i.e., 10^{13} < 'metabolic' number < 10^{16}, and 0.72 < 'DO saturation' number < 0.97). The contrasting characteristic of the high and low metabolism regimes was apparent, respectively, by their most and least favorable environmental condition for stream DO depletion—through reduced dissolution and reaeration, alongside increased respiration. The emergent process diagram led to a generalized power law scaling relationship of the 'DO saturation' number as a function of the 'metabolic' number (exponent ~ 1/3; NSE = 0.83–0.85, RSR = 0.39–0.40). The metabolic scaling relationship was leveraged to develop a generalized empirical model to successfully predict DO in diverse streams across the U.S. Atlantic Coast (NSE = 0.83, RSR = 0.41). The findings from the study supported the underlying research hypothesis that DO represents emergent 'biogeochemical' similitude and scaling relationship across diverse coastal streams. The emergent process diagram, metabolic scaling law, and generalized prediction model of DO would help understand and manage water quality and ecosystem health of coastal streams in the U.S. and elsewhere.

Notations

The following notations and symbols were used in this paper:

P_a	atmospheric pressure
T_W	water temperature
c_p	specific heat of water
TP	total phosphorus
S	salinity
W	stream width
D	stream depth
Q	stream flow
DO	dissolved oxygen
DO_{sat}	saturated dissolved oxygen
P_{25}	25th percentile
P_{75}	75th percentile
IQR	interquartile range
M, L, T, K	dimensions of mass, length, time, and temperature, respectively.
Π_i	dimensionless numbers (i = 1, 2, 3, 4, 5, and 6)
f, φ, ψ	functions
a, b, c, d	exponents of power law Eq. (3)
α, β	model parameters of Eq. (16)

CRediT authorship contribution statement

O.I. Abdul-Aziz generated the research idea, conceptualized the methodology, and provided initial formulations and empirical evidence as the proof of concept. S. Ahmed worked with O.I. Abdul-Aziz as a graduate research assistant to arrive at the final formulations and results. Both authors contributed to the writing of the manuscript. O.I. Abdul-Aziz administered the sponsored project and supervised S. Ahmed. All authors have read and agreed to the published version of the manuscript.

Declaration of competing interest

The authors declare that they have no known competing financial interests or personal relationships that could have appeared to influence the work reported in this paper.

Acknowledgments

The research was funded by the U.S. National Science Foundation (NSF) CAREER Award to Dr. Omar I. Abdul-Aziz (NSF CBET Environmental Sustainability Award Number 1561942/1454435). The findings and conclusions of this research are those of the authors, and do not necessarily reflect the views of NSF.

Appendix A. Supplementary data

Supplementary data to this article can be found online at https://doi.org/10.1016/j.scitotenv.2022.153292.

References

Abdul-Aziz, O.I., Ahmed, S., 2017. Relative linkages of stream water quality and environmental health with the land use and hydrologic drivers in the coastal-urban watersheds of Southeast Florida. GeoHealth 1, 180–195. https://doi.org/10.1002/2017GH000058.

Abdul-Aziz, O.I., Ahmed, S., 2019. Evaluating the emergent controls of stream water quality with similitude and dimensionless numbers. J. Hydrol. Eng. 24, 04019010. https://doi.org/10.1061/(asce)he.1943-5584.0001769.

Appling, A.P., Read, J.S., Winslow, L.A., Arroita, M., Bernhardt, E.S., Griffiths, N.A., Hall, R.O., Harvey, J.W., Heffernan, J.B., Stanley, E.H., Stets, E.G., Yackulic, C.B., 2018. Data descriptor: the metabolic regimes of 356 rivers in the United States. Sci. Data 5, 1–14. https://doi.org/10.1038/sdata.2018.292\.

Arsenault, R., Brissette, F.P., 2014. Continuous streamflow prediction in ungauged basins: the effects of equifinality and parameter set selection on uncertainty in regionalization approaches. Water Resour. Res. 50, 6135–6153. https://doi.org/10.1002/2013WR014898.

Bennett, J.P., Rathbun, R.E., 1972. Reaeration in open-channel flow. Geological Survey Professional Paper, Washington.

Berger, E., Frör, O., Schäfer, R.B., 2019. Salinity impacts on river ecosystem processes: a critical mini-review. Philos. Trans. R. Soc. B Biol. Sci. 374. https://doi.org/10.1098/rstb.2018.0010.

Bernhardt, E.S., Heffernan, J.B., Grimm, N.B., Stanley, E.H., Harvey, J.W., Arroita, M., Appling, A.P., Cohen, M.J., McDowell, W.H., Hall Jr., R.O., Read, J.S., Roberts, B.J., States, E.G., Yackulic, C.B., 2018. The metabolic regimes of flowing waters. Limnol. Oceanogr. 63 (S1), S99–S118. https://doi.org/10.1002/lno.10726.

Beven, K., Binley, A., 1992. The future of distributed models: model calibration and uncertainty prediction. Hydrol. Process. 6, 279–298. https://doi.org/10.1002/HYP.3360060305.

Beven, K., Freer, J., 2001. Equifinality, data assimilation, and uncertainty estimation in mechanistic modelling of complex environmental systems using the GLUE methodology. J. Hydrol. 249, 11–29. https://doi.org/10.1016/S0022-1694(01)00421-8.

Blaszczak, J.R., Delesantro, J.M., Urban, D.L., Doyle, M.W., Bernhardt, E.S., 2019. Scoured or suffocated: urban stream ecosystems oscillate between hydrologic and dissolved oxygen extremes. Limnol. Oceanogr. 64, 877–894. https://doi.org/10.1002/lno.11081.

Chapra, S.C., 2008. Surface water-quality modeling. Waveland press, Long Grove, Illinois.

Correa-González, J.C., Cortés, J.A., Pérez-Munguía, R.M., Chávez-Parga, M.del C., 2014. Photosynthesis, respiration and reaeration in a stream with complex dissolved oxygen pattern and temperature dependence. Ecol. Modell. 273, 220–227. https://doi.org/10.1016/j.ecolmodel.2013.11.018.

Diamantini, E., Lutz, S.R., Mallucci, S., Majone, B., Merz, R., Bellin, A., 2018. Driver detection of water quality trends in three large european river basins. Sci. Total Environ. 612, 49–62. https://doi.org/10.1016/j.scitotenv.2017.08.172.

Dick, J.J., Soulsby, C., Birkel, C., Malcolm, I., Tetzlaff, D., 2016. Continuous dissolved oxygen measurements and modelling metabolism in Peatland Streams. PLOS One 11, 1–23. https://doi.org/10.1371/journal.pone.0161363.

Dodds, W.K., 2006. Nutrients and the "dead zone": the link between nutrient ratios and dissolved oxygen in the northern Gulf of Mexico. Front. Ecol. Environ. 4 (4), 211–217. https://doi.org/10.1890/1540-9295(2006)004[0211:NATDZT]2.0.CO;2.

Dodds, W.K., Smith, V.H., 2016. Nitrogen, phosphorus, and eutrophication in streams. Inl. Waters 6, 155–164. https://doi.org/10.5268/IW-6.2.909.

Entrekin, S.A., Clay, N.A., Mogilevski, A., Howard-Parker, B., Evans-White, M.A., 2019. Multiple riparian–stream connections are predicted to change in response to salinization. Phil. Trans. R. Soc. B. 374. https://doi.org/10.1098/rstb.2018.0042.

Ferreira, V., Chauvet, E., 2011. Synergistic effects of water temperature and dissolved nutrients on litter decomposition and associated fungi. Glob. Chang. Biol. 17, 551–564. https://doi.org/10.1111/j.1365-2486.2010.02185.x.

Finnemore, E.J., Franzini, J.B., 2002. Fluid mechanics with engineering applications. 10th edition. McGraw-Hill, New York.

Garcia, H.E., Gordon, L.I., 1992. Oxygen solubility in seawater: better fitting equations. Limnol. Oceanogr. 37 (6), 1307–1312. https://doi.org/10.4319/lo.1992.37.6.1307.

Girard, J., 2013. Principles of environmental chemistry. Jones & Bartlett Publishers.

Gonçalves, J.C.D.S.I., Silveira, A., Júnior, G.B.L., Da Luz, M.S., Simões, A.L.A., 2017. Reaeration coefficient estimate: new parameter for predictive equations. Water Air Soil Pollut. 228. https://doi.org/10.1007/s11270-017-3491-5.

Gu, N., Song, Q., Yang, X., Yu, X., Li, X., Li, G., 2020. Fluorescence characteristics and biodegradability of dissolved organic matter (DOM) leached from non-point sources in southeastern China. Environ. Pollut. 258, 113807. https://doi.org/10.1016/j.envpol.2019.113807.

Hager, W.H., 2018. Bed-load transport: advances up to 1945 and outlook into the future. J. Hydraul. Res. 56 (5), 596–607. https://doi.org/10.1080/00221686.2017.1405370.

Hondzo, M., Voller, V.R., Morris, M., Foufoula-Georgiou, E., Finlay, J., Ganti, V., Power, M.E., 2013. Estimating and scaling stream ecosystem metabolism along channels with heterogeneous substrate. Ecohydrology 6 (4), 679–688. https://doi.org/10.1002/eco.1391.

Jabiol, J., Gossiaux, A., Lecerf, A., Rota, T., Guérold, F., Danger, M., Poupin, P., Gilbert, F., Chauvet, E., 2020. Variable temperature effects between heterotrophic stream processes and organisms. Freshw. Biol. 65 (9), 1543–1554. https://doi.org/10.1111/fwb.13520.

Jacobs, J., Rhodes, M., Sturgis, B., Wood, B., 2009. Influence of environmental gradients on the abundance and distribution of mycobacterium spp. In a coastal lagoon estuary. Appl. Environ. Microbiol. 75 (23), 7378–7384. https://doi.org/10.1128/AEM.01900-09.

Jalali, M., Jalali, M., 2017. Assessment risk of phosphorus leaching from calcareous soils using soil test phosphorus. Chemosphere 171, 106–117. https://doi.org/10.1016/j.chemosphere.2016.12.042.

Järvenpää, M., Pauli, B.D., Lindström, K., 2019. Water turbidity constrains male mating success in a marine fish. Behav. Ecol. Sociobiol. 73 (10), 1–7. https://doi.org/10.1007/s00265-019-2752-2.

Johannsson, O.E., Ferreira, M.S., Smith, D.S., Wood, C.M., Val, A.L., 2021. Interplay of oxygen and light in the photo-oxidation of dissolved organic carbon. Water Res. 201, 117332. https://doi.org/10.1016/j.watres.2021.117332.

Kadlec, R.H., Reddy, K.R., 2001. Temperature effects in treatment wetlands. Water Environ. Res. 73 (5), 543–557. https://doi.org/10.2175/106143001X139614.

Keenleyside, W., 2019. Microbiology: Canadian edition. 1st edition. Pressbooks.

Kindley, S., 2021. Linking urban land use to aquatic metabolic regimes. Retrieved fromDuke University, Master's project. https://hdl.handle.net/10161/22701.

Koenig, L.E., Helton, A.M., Savoy, P., Bertuzzo, E., Heffernan, J.B., Hall, R.O., Bernhardt, E.S., 2019. Emergent productivity regimes of river networks. Limnol. Oceanogr. Lett. 4, 173–181. https://doi.org/10.1002/LOL2.10115.

Kundu, P.K., Cohen, I.M., 2002. Fluid mechanics. 2nd edition. Elsevier Academic Press, California.

Kundu, P.K., Cohen, I.M., 2004. Fluid mechanics. 3rd edition. Elsevier Academic Press, New York.

Ledford, S.H., Diamond, J.S., Toran, L., 2021. Large spatiotemporal variability in metabolic regimes for an urban stream draining four wastewater treatment plants with implications for dissolved oxygen monitoring. PLoS One 16, e0256292. https://doi.org/10.1371/journal.pone.0256292.

Li, X., Sha, J., Wang, Z.L., 2017. A comparative study of multiple linear regression, artificial neural network and support vector machine for the prediction of dissolved oxygen. Hydrol. Res. 48 (5), 1214–1225. https://doi.org/10.2166/nh.2016.149.

Mahaffey, C., Palmer, M., Greenwood, N., Sharples, J., 2020. Impacts of climate change on dissolved oxygen concentration relevant to the coastal and marine environment around the UK. MCCIP Sci. Rev. 2002, 31–53. https://doi.org/10.14465/2020.arc02.oxy.

Martinez-Villalobos, C., Neelin, J.D., 2018. Shifts in precipitation accumulation extremes during the warm season over the United States. Geophys. Res. Lett. 45, 8586–8595. https://doi.org/10.1029/2018GL078465.

Miragliotta, G., 2011. The power of dimensional analysis in production systems design. Int. J. Prod. Econ. 131 (1), 175–182. https://doi.org/10.1016/j.ijpe.2010.08.009.

Mitsuo, Y., 2017. Determining the relative importance of catchment- and site-scale factors in structuring fish assemblages in small coastal streams. Knowl. Manag. Aquat. Ecosyst. 418, 57. https://doi.org/10.1051/kmae/2017046.

Moriasi, D.N., Arnold, J.G., Van Liew, M.W., Bingner, R.L., Harmel, R.D., Veith, T.L., 2007. Model evaluation guidelines for systematic quantification of accuracy in watershed simulations. Trans. ASABE 50 (3), 885–900. https://doi.org/10.13031/2013.23153.

National Solar Radiation Data Base (NSRDB), 2017. . Available online at https://maps.nrel.gov/nsrdb-viewer/. (Accessed 15 January 2017).

National Water Quality Monitoring Council (NWQMC), 2017. . Available online at https://www.waterqualitydata.us/portal. (Accessed 1 October 2017).

Ni, W., Li, M., Ross, A.C., Najjar, R.G., 2019. Large projected decline in dissolved oxygen in a eutrophic estuary due to climate change. J. GeophysRes. Oceans 124 (11), 8271–8289. https://doi.org/10.1029/2019JC015274.

Omernik, J.M., Griffith, G.E., 2014. Ecoregions of the conterminous United States: evolution of a hierarchical spatial framework. Environ. Manag. 54 (6), 1249–1266.. https://10.1007/s00267-014-0364-1.

Poikane, S., Várbíró, G., Kelly, M.G., Birk, S., Phillips, G., 2021. Estimating river nutrient concentrations consistent with good ecological condition: more stringent nutrient thresholds needed. Ecol. Indic. 121, 107017. https://doi.org/10.1016/j.ecolind.2020.107017.

Putro, B., Kjeldsen, T.R., Hutchins, M.G., Miller, J., 2016. An empirical investigation of climate and land-use effects on water quantity and quality in two urbanising catchments in the southern United Kingdom. Sci. Total Environ. 548, 164–172. https://doi.org/10.1016/j.scitotenv.2015.12.132.

Romeijn, P., Comer-Warner, S.A., Ullah, S., Hannah, D.M., Krause, S., 2019. Streambed organic matter controls on carbon dioxide and methane emissions from streams. Environ. Sci. Technol. 53 (5), 2364–2374. https://doi.org/10.1021/acs.est.8b04243.

Rosenfeld, J.S., Macdonald, S., Foster, D., Amrhein, S., Bales, B., Williams, T., Race, F., Livingstone, T., 2002. Importance of small streams as rearing habitat for coastal cutthroat trout. N. Am. J. Fish Manag. 22, 177–187. https://doi.org/10.1577/1548-8675(2002)022<0177:IOSSAR>2.0.CO;2.

Savoy, P., Appling, A.P., Heffernan, J.B., Stets, E.G., Read, J.S., Harvey, J.W., Bernhardt, E.S., 2019. Metabolic rhythms in flowing waters: an approach for classifying river productivity regimes. Limnol. Oceanogr. 64, 1835–1851. https://doi.org/10.1002/lno.11154.

Schaefer, S.C., Hollibaugh, J.T., 2017. Temperature decouples ammonium and nitrite oxidation in coastal waters. Environ. Sci. Technol. 51 (6), 3157–3164. https://doi.org/10.1021/acs.est.6b03483.

Schemel, L.E., 2001. Simplified conversions between specific conductance and salinity units for use with data from monitoring stations. Interagency Ecol. Prog. Newslett. 14 (1), 17–18.

Schwefel, R., Hondzo, M., Wüest, A., Bouffard, D., 2017. Scaling oxygen microprofiles at the sediment interface of deep stratified waters. Geophys. Res. Lett. 44 (3), 1340–1349. https://doi.org/10.1002/2016GL072079.

Segatto, P.L., Battin, T.J., Bertuzzo, E., 2021. The metabolic regimes at the scale of an entire stream network unveiled through sensor data and machine learning. Ecosystems https://doi.org/10.1007/s10021-021-00618-8.

Shrestha, S., Kazama, F., 2007. Assessment of surface water quality using multivariate statistical techniques: a case study of the Fuji river basin, Japan. Environ. Modell. Softw. 22 (4), 464–475. https://doi.org/10.1016/j.envsoft.2006.02.001.

Thuesen, P.A., Ebner, B.C., Larson, H., Keith, P., Silcock, R.M., Prince, J., Russell, D.J., 2011. Amphidromy links a newly documented fish community of continental australian streams, to oceanic islands of the west pacific. PLoS One 6. https://doi.org/10.1371/journal.pone.0026685.

Tukey, J.W., 1977. Exploratory data analysis. Addison-Wesley, Reading, MA.

Tyler, R.M., Brady, D.C., Targett, T.E., 2009. Temporal and spatial dynamics of diel-cycling hypoxia in estuarine tributaries. Estuar. Coasts 32 (1), 123–145. https://doi.org/10.1007/s12237-008-9108-x.

U.S. Environmental Protection Agency (USEPA), 1986. Quality criteria for water 1986. U.S. Environmental Protection Agency, Washington, D.C. Report 440/5-86-001.

United States Geological Survey (USGS), 2017. National water information system. Available online at https://maps.waterdata.usgs.gov/mapper/index.html. (Accessed 17 November 2017).

United States Geological Survey (USGS), 2018. Land cover change in the Eastern United States. Available online at https://landcovertrends.usgs.gov/east/regionalSummary.html. (Accessed 1 January 2018).

van Dael, T., De Cooman, T., Smolders, E., 2020. In-stream oxygenation to mitigate internal loading of phosphorus in lowland streams. J. Hydrol. 590, 125536. https://doi.org/10.1016/j.jhydrol.2020.125536.

Wan, Y., Qian, Y., Migliaccio, K.W., Li, Y., Conrad, C., 2014. Linking spatial variations in water quality with water and land management using multivariate techniques. J. Environ. Qual. 43 (2), 599–610. https://doi.org/10.2134/jeq2013.09.0355.

Wang, P., Linker, L.C., 2009. Assessment of nitrogen and phosphorus control trade-offs using a water quality model with a response surface method. J. Water Resour. Plan. Manag. 135 (3), 171–177. https://doi.org/10.1061/(ASCE)0733-9496(2009)135:3(171).

Wang, J., Lü, G., Guo, X., Wang, Y., Ding, S., Wang, D., 2015. Conservation tillage and optimized fertilization reduce winter runoff losses of nitrogen and phosphorus from farmland in the Chaohu Lake region, China. Nutr. Cycl. Agroecosyst. 101 (1), 93–106. https://doi.org/10.1007/s10705-014-9664-3.

Warnaars, T.A., Hondzo, M., Power, M.E., 2007. Abiotic controls on periphyton accrual and metabolism in streams: scaling by dimensionless numbers. Water Resour. Res. 43, W08425. https://doi.org/10.1029/2006WR005002.

Wurtsbaugh, W.A., Paerl, H.W., Dodds, W.K., 2019. Nutrients, eutrophication and harmful algal blooms along the freshwater to marine continuum. Wiley interdiscip. Rev. Water. 6 (5), e1373. https://doi.org/10.1002/wat2.1373.

Xu, Z., Xu, Y.J., 2016. A deterministic model for predicting hourly dissolved oxygen change: development and application to a shallow eutrophic lake. Water 8 (2), 41. https://doi.org/10.3390/w8020041.

Yu, L., Zhong, S., Pei, L., Bian, X., Heilman, W.E., 2016. Contribution of large-scale circulation anomalies to changes in extreme precipitation frequency in the United States. Environ. Res. Lett. 11. https://doi.org/10.1088/1748-9326/11/4/044003.

Yuan, X., Li, S., Hu, J., Yu, M., Li, Y., Wang, Z., 2019. Experiments and numerical simulation on the degradation processes of carbamazepine and triclosan in surface water: a case study for the Shahe Stream, South China. Sci. Total Environ. 655, 1125–1138. https://doi.org/10.1016/j.scitotenv.2018.11.290.

Zeleňáková, M., Čarnogurská, M., Šlezingr, M., Słyś, D., Purcz, P., 2013. A model based on dimensional analysis for prediction of nitrogen and phosphorus concentrations at the river station Ižkovce, Slovakia. Hydrol. Earth Syst. Sci. 17 (1), 201–209. https://doi.org/10.5194/hess-17-201-2013.

Zhang, J.Z., Huang, X.L., 2011. Effect of temperature and salinity on phosphate sorption on marine sediments. Environ. Sci. Technol. 45 (16), 6831–6837. https://doi.org/10.1021/es200867p.

Zhang, Y., Fitch, P., Vilas, M.P., Thorburn, P.J., 2019. Applying multi-layer artificial neural network and mutual information to the prediction of trends in dissolved oxygen. Front. Environ. Sci. 7, 46. https://doi.org/10.3389/fenvs.2019.00046.

Zhi, W., Feng, D., Tsai, W.P., Sterle, G., Harpold, A., Shen, C., Li, L., 2021. From hydrometeorology to river water quality: can a deep learning model predict dissolved oxygen at the continental Scale? Environ. Sci. Technol. 55 (4), 2357–2368. https://doi.org/10.1021/acs.est.0c06783.